ACS APPLIED MATERIALS & INTERFACES

RESEARCH ARTICLE

www.acsami.org

Polymer Brush Guided Formation of Thin Gold and Palladium/Gold Bimetallic Films

Dusko Paripovic and Harm-Anton Klok*

École Polytechnique Fédérale de Lausanne (EPFL), Institut des Matériaux and Institut des Sciences et Ingénierie Chimiques, Laboratoire des Polymères, Bâtiment MXD, Station 12, CH-1015 Lausanne, Switzerland.

Supporting Information

ABSTRACT: This manuscript reports a new strategy to guide the chemical solution deposition of thin, microstructured metal films. The proposed strategy is based on the use of poly(2-(methacryloyloxy)ethyl ammonium chloride) (PMETAC) brushes grown via surface-initiated atom transfer radical polymerization as a template. Thin gold films have been prepared by first loading the PMETAC brushes with $HAuCl_4$, followed by a $NaBH_4$ mediated reduction to produce a PMETAC-gold nanoparticle composite film and finally an oxygen plasma treatment to remove the stabilizing polymer brush matrix and generate the desired thin gold film. The thickness of the gold films was found to scale with the thickness of the PMETAC brush template. This approach can also be extended to more complex, bimetallic films by exposing the PMETAC template successively to two different precursor salts. In this way, gradient type bimetallic palladium/gold films could be prepared.

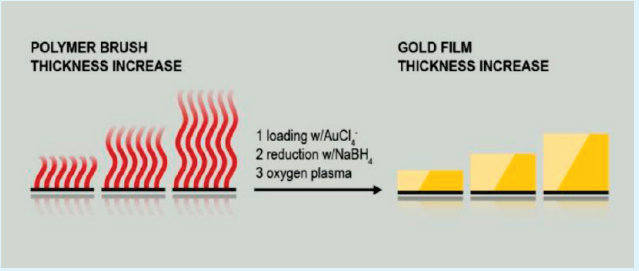

KEYWORDS: polymer brushes, surface-initiated atom transfer radical polymerization, template, polymer-assisted deposition, gold film, bimetallic films, gradient film

INTRODUCTION

Thin metal and metal oxide films are of great technological importance and find use in a broad range of applications including catalysis,[1] corrosion protection,[2] microelectronics,[3−5] sensing,[6,7] as well as fuel[8] and solar cells.[9] Such films are typically produced by physical or chemical vapor deposition methods, such as e-beam or thermal evaporation, cathodic arc technology, or galvanic methods.[10−16] Although these techniques generally work well, they also have some limitations. On the one hand, these are related to the necessary equipment, which can be costly. On the other hand, often only relatively small area films can be produced and it can be challenging to fabricate films with complex micro/nanostructures. To overcome some of these issues, there has been an increasing interest in the use of chemical-solution deposition techniques to produce thin metal and metal oxide films. Examples of methods that have been successfully used include electroless plating,[17−20] sol−gel,[21] nanoparticle-based solution deposition,[22−24] and polymer-assisted deposition.[25,26]

Chemical-solution deposition of thin metal and metal oxide films can be carried out on unmodified substrates, but sometimes also involves the application of a thin alkoxysilane or polymer coating to improve adhesion between the metal(oxide) film and the underlying substrate.[27,28] An interesting conceptual extension of these later approaches would be to use the thin organic/polymer coating not merely to improve adhesion, but also to control film growth both laterally as well as in terms of thickness. Among the different strategies that are available to prepare thin polymer coatings, surface-initiated controlled radical polymerization (SI-CRP) techniques are particularly attractive. SI-CRP results in polymer films that are also referred to as polymer brushes. Polymer brushes consist of a densely packed arrangement of polymer chains that are covalently attached to the underlying substrate via one of the chains ends. SI-CRP is attractive because the "living"/controlled nature of these polymerization reactions allows precise growth over brush thickness (typically ∼10−300 nm), composition, and architecture.[29]

The use of polymer brushes to template the chemical solution fabrication of thin nonmetallic, inorganic films has been demonstrated in a number of recent papers. Choi et al., for example, have used poly(*N*,*N*-dimethylaminoethyl methacrylate) (PDMAEMA) brushes to guide the formation of thin micropatterned titanium dioxide[30] and silica films.[31,32] These authors could demonstrate that the thickness of the silica films could be controlled by the thickness of the PDMAEMA brush and that silification on patterned brush substrates only occurred at PDMAEMA presenting areas. A similar approach has been used to prepare microstructured calcite films using patterned poly(methacrylic acid) brushes as a template.[33] In a number of publications, the use of polymer brushes as matrices for the synthesis of metal nanoparticles has been demonstrated.[34−39] Generally, the preparation of these polymer brush-metal nanocomposite films involves loading of a polyelectrolyte brush with an appropriate metal precursor salt followed by a wet chemical reduction.

Received: December 23, 2010
Accepted: February 14, 2011
Published: March 07, 2011

In this process, the polymer brush has multiple functions: (i) it acts as a matrix that can be loaded with precursor ions; (ii) it allows the immobilization of the resulting nanoparticles and prevents their aggregation and (iii) it serves as a capping agent to limit nanoparticle growth. The interest in these polymer brush−metal nanocomposite films is due to the unusual or new optical, catalytic, and mechanical properties that can be endowed by the metal nanoparticles in combination with the possibilities offered by the polymer brush to introduce responsiveness to external stimuli such as temperature or ionic strength. The work described in this manuscript builds upon these previous investigations and explores the use of polymer brushes as matrices to template the formation of thin metallic, here, gold films rather than nanoparticle assemblies. While polymer brushes have been used to immobilize catalysts that were subsequently used for the electroless deposition of copper,[19] we are not aware of any prior reports that describe the direct polymer brush templated synthesis of thin metal films. The aim of this manuscript is to explore the feasibility of polymer brushes grown via surface-initiated atom transfer radical polymerization to act as templates to guide the formation of thin gold films. Specifically, the following questions will be addressed: (i) can the height and lateral dimensions of the gold films be controlled by varying brush thickness and using micropatterned brush substrates? (ii) is it possible to utilize the defined geometrically controlled microenvironment of the brush template to generate more complex, e.g., bimetallic, films?

EXPERIMENTAL SECTION

Materials. *N,N*-Dimethylaminoethyl methacrylate (DMAEMA) (98%), copper(I)bromide (99.995+ %), iodomethane (99%), 2,2′-bipyridyl (≥99%), NaCl, gold(III)chloride hydrate ($HAuCl_4$ > 52% Au, ACS grade), sodium tetrachloropalladate(II) (98%), sodium borohydride (99%), 5-hexen-1-ol (>98%), 2-bromo-2-methylpropionyl bromide (98%), chlorodimethylsilane (98%), and Pt/C (10% Pt) were purchased from Sigma Aldrich and used as received unless specified otherwise. All organic solvents used for washing were technical grade. Inhibitor was removed from DMAEMA by passage through a column of basic alumina. Ultra high quality water with a resistance of 18.2 MΩ cm (at 25 °C) was obtained from a Millipore Milli-Q gradient machine fitted with a 0.22 μm filter. Silicon (100) covered with a native silicon oxide layer and Pyrex slides (both 10 mm × 7 mm) were used as substrates for surface-initiated polymerization.

Methods. Prior to initiator immobilization and surface-initiated polymerization, substrates were cleaned using a Tepla 300 microwave induced plasma system (PVA Tepla AG, Germany). The cleaning process lasted 4 min at 500 W with an oxygen flow rate of 400 mL/min. Up to six 4 min long cycles were applied. Atomic force microscopy was performed on a Veeco CP-II instrument (Digital instruments, Santa Barbara, CA) in tapping mode using a MPP-11123−10 (Veeco) cantilever. To determine layer thicknesses, cross-sectional height profiles of micropatterned polymer brushes and gold films were recorded. X-ray photoelectron spectroscopy (XPS) was carried out on the non-micropatterned area of a polymer brush or gold-coated silicon substrate using an Axis Ultra instrument from Kratos Analytical equipped with a conventional hemispheric analyzer. The X-ray source employed was a monochromatic Al Kα (1486.6 eV) source operated at 100 W and 1 × 10^{-9} mbar. Static water contact angles were determined using a DataPhysics OCA 35 goniometer on the nonpatterned part of a polymer brush coated substrate. FTIR spectroscopy was performed on a Nicolet Magna-IR 560 spectrometer equipped with a nitrogen purged 45° angle micro specular reflectance accessory (Specac Ltd., UK). The measurements were carried out on nonpatterned areas of polymer brush coated silicon wafers. An ATRP initiator coated silicon wafer was used as a background. UV/Visible absorbance spectra were obtained on a Varian Cary 100 Bio instrument operating at 25 °C. Spectra were recorded on polymer brush or gold films supported on Pyrex substrates, which were placed upright against the wall of an UV cuvette. A clean Pyrex wafer was used as the background. TEM investigations of cross-sectioned gold and palladium/gold films were performed on a PHILIPS CM300 instrument equipped with energy-dispersive X-ray (EDX) spectroscopy. The films were prepared by Tripod mechanical polishing followed by ion milling (PIPS (Precision Ion Polishing System) from Gatan).

Procedures. ATRP initiator modified substrates were prepared by immobilization of 6-(chlorodimethylsilyl)hexyl 2-bromo-2-methylpropanoate, which was synthesized and subsequently immobilized on silicon and Pyrex substrates following a literature procedure.[40]

Micropatterned polymer brushes were obtained by UV irradiation of ATRP initiator modified substrates using a TEM grid as a photomask.[33] Each silicon wafer was divided in two parts. One half of the ATRP initiator modified slide was covered by a clean silicon substrate and therefore protected from the irradiation. After surface-initiated polymerization, this part of the substrate, which is covered with a uniform, nonpatterned polymer brush layer, was used for water contact angle, XPS, UV−vis and FTIR analysis. On the other half of the wafer, a TEM grid was placed in order to form a micropatterned area. Substrates were placed 4 cm away from the Hamamatsu UV lamp source (Lightningcure L8858) and irradiated for 5 min.

Preparation of Poly(2-(methacryloyloxy)ethyl ammonium chloride) (PMETAC) Brushes. First, PDMAEMA brushes were grown following the literature procedure from Choi and co-workers[31] using: DMAEMA (1.5722 g, 10 mmol), CuBr (0.0143 g, 0.1 mmol), 2,2′-bipyridyl (0.0312 g, 0.2 mmol) and 10 mL of water. After that, the resulting polymer brushes were quaternized using a 10 vol% solution of methyl iodide in acetone overnight[41] and subsequently rinsed with acetone, ethanol, 500 mM NaCl, and then again with water, ethanol and dried under a flow of air to afford desired PMETAC brushes. As an alternative (but not explored here), PMETAC brushes can also be prepared via direct surface-initiated atom transfer radical polymerization of 2-(methacryloyloxy)ethyl ammonium chloride, which is commercially available.[19,34]

Tetrachloroaurate(III) ($AuCl_4^-$) or Tetrachloropalladate(II) ($PdCl_4^{2-}$) Loaded Polymer Brushes. These were obtained by incubating PMETAC covered substrates in a filtered 1 mg/mL aqueous solution of tetrachloroauric acid or sodium tetrachloropalladate(II) for 30 min. After incubation, the slides were quickly rinsed with water and dried under a flow of air. For the preparation of bimetallic palladium/gold films, the $PdCl_4^{2-}$ loaded PMETAC brushes were exposed to a 1 mg/mL aqueous solution of tetrachloroauric acid for 2 h and subsequently quickly rinsed with water and dried under a flow of air.

Reduction with $NaBH_4$. $AuCl_4^-$ loaded polymer brushes were immersed for 30 s in freshly prepared 10, 100, or 500 mM aqueous sodium borohydride solutions. For the reduction of $PdCl_4^{2-}$/$AuCl_4^-$ loaded brushes, a 100 mM aqueous sodium borohydride solution was used. After removal from the sodium borohydride solutions, the slides were rinsed with water and dried with an air stream.

Gold Films. These were prepared by oxygen plasma treatment of polymer brush-gold nanoparticle composite films. The plasma treatment was typically performed in 4−6 cycles of 4 min each at 500 W and oxygen flow of 400 mL/min

Palladium/Gold Gradient Films. These were created by 6 oxygen plasma treatment cycles of polymer brush−palladium/gold nanoparticle composite films using the same plasma treatment conditions as for the gold films.

RESULTS AND DISCUSSION

Scheme 1 outlines the proposed strategy for the polymer brush guided formation of thin gold films. The process starts with the formation of a poly(2-(methacryloyloxy)ethyl ammonium chloride) (PMETAC) brush via surface-initiated atom transfer

Scheme 1. Polymer Brush Guided Formation of Thin Gold Films

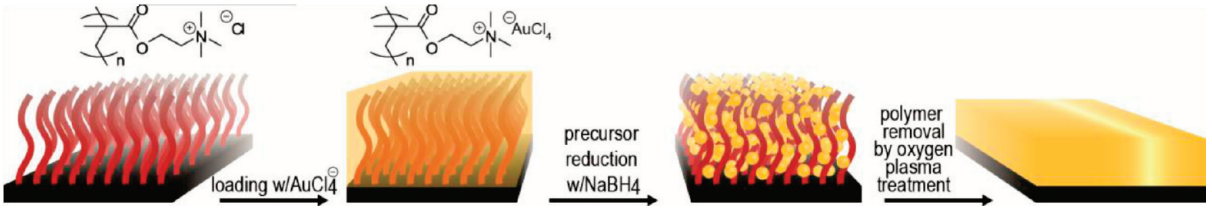

Table 1. Film Thicknesses of Patterned PDMAEMA, PMETAC, and PMETAC·$AuCl_4$ Brushes As Determined from AFM Cross-Sectional Analysis

	thickness (nm)		
polymerization time (min)	PDMAEMA	PMETAC	PMETAC·$AuCl_4$
8	37	54	55
30	99	150	162
240	285	315	355

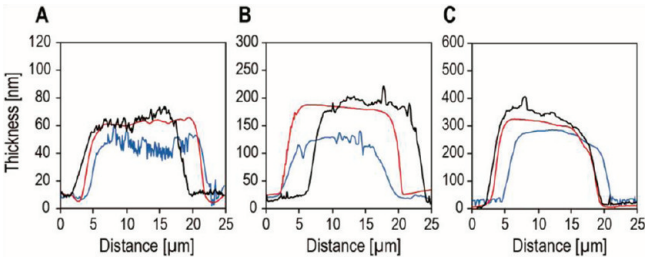

Figure 1. AFM cross-sectional profiles of patterned PDMAEMA (blue), PMETAC (red) and PMETAC•$AuCl_4$ (black) polymer brushes. The PMETAC and PMETAC·$AuCl_4$ brushes were prepared from PDMAEMA brushes with initial thicknesses of: (A) 37, (B) 99, and (C) 285 nm.

radical polymerization. The PMETAC brush is subsequently loaded with $HAuCl_4$ and treated with $NaBH_4$ to generate a polymer brush-gold nanoparticle (AuNP) composite film. Finally, these composite films are exposed to an oxygen plasma, which serves to simultaneously remove the stabilizing PMETAC brush matrix and induce coalescence of the gold nanoparticles into a thin film.[42]

The synthesis of the PMETAC brushes starts with the SI-ATRP of N,N-dimethylaminoethyl methacrylate (DMAEMA), which was performed using a published protocol.[31] Brushes were grown from substrates that were subdivided into two parts. One part was uniformly covered and was used for FTIR and XPS analysis. The other half was covered with a micropatterned brush and was used for atomic force microscopy analysis to determine the thickness of the polymer brushes and the corresponding nanocomposite films and gold films. By varying the polymerization time, PDMAEMA brushes with thicknesses of 37, 99, and 285 nm were obtained (Table 1, Figure 1). In a subsequent step, the PDMAEMA brushes were treated with MeI[41] and subsequently washed with an aqueous solution of NaCl to generate the desired PMETAC brushes. Quaternization of the PDMAEMA brushes resulted in a significant increase in film thickness (Table 1) as well as in a decrease of the static water contact angle from 48.3° (PDMAEMA) to 33.5° (PMETAC). The conversion of the PDMAEMA brushes to PMETAC brushes was further followed with FTIR spectroscopy (Figure 2) and

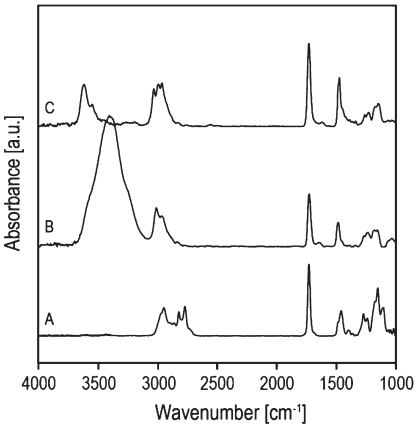

Figure 2. FTIR spectra of: (A) PDMAEMA (99 nm), (B) PMETAC (150 nm), and (C) PMETAC·$AuCl_4$ (162 nm) brushes.

XPS analysis (Figure 3). The complete disappearance of the symmetric $-CH_3$ stretching vibration bands at 2769 and 2820 cm^{-1} in the spectra of the PDMAEMA brush suggests quantitative quaternization of the tertiary amine groups.[43] Comparison of the XPS spectra, and in particular the N1s and Cl2p high resolution scans, provides further evidence for the successful quaternization. Quaternization results in appearance of a Cl2p signal at about 200 eV as well as in a shift of N1s signal from 397.7 to 401 eV. The N1s high resolution scan of PMETAC brush shows a small signal at 397.7 eV, indicating that there is a minor residual fraction of nonquaternized tertiary amine groups (~10%). Quaternization of the PDMAEMA brush is also accompanied by hydration of the surface-tethered polymer film, as evidenced by a broad OH stretching band at 3200−3700 cm^{-1} in the FTIR spectrum. Furthermore, the XPS O1s high-resolution scan also reveals an additional signal at 530.8 eV, which we tentatively attribute to hydration water. The survey scan of the PMETAC brush also shows a Na signal, which is due to a nonoptimized rinsing procedure and residual Na^+ in the polymer layer.

The first step in the polymer brush guided preparation of thin gold films consists of loading the PMETAC coated substrates with the precursor salt ($HAuCl_4$). This process can be followed using a number of techniques. As shown in Figure 4, the UV/vis spectra of the $AuCl_4^-$-loaded brushes reveal a characteristic absorption at 320 nm, which is due to the absorbance of the $AuCl_4^-$. The intensity of this band increases with increasing brush thickness, which reflects the higher loading capacity of the thicker brushes. Loading the PMETAC brushes with $HAuCl_4$ also results in drastic changes in the wetting properties of the substrates. For a 150 nm thick PMETAC brush, for example, the static water contact angle increased from 33.5 to 67.6° upon loading the brush with $HAuCl_4$. FTIR analysis revealed that this process was accompanied by dehydration of the polymer brush,

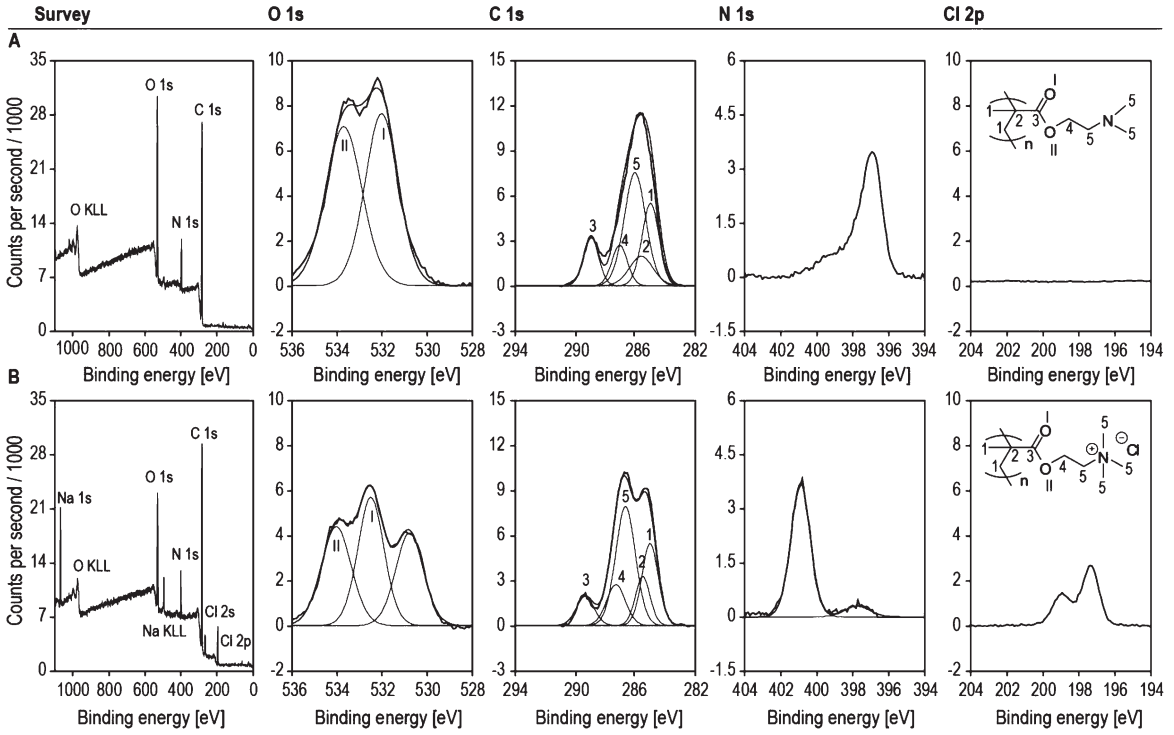

Figure 3. XPS survey and high-resolution spectra of (A) a 99 nm thick PDMAEMA and (B) a 150 nm thick PMETAC brush.

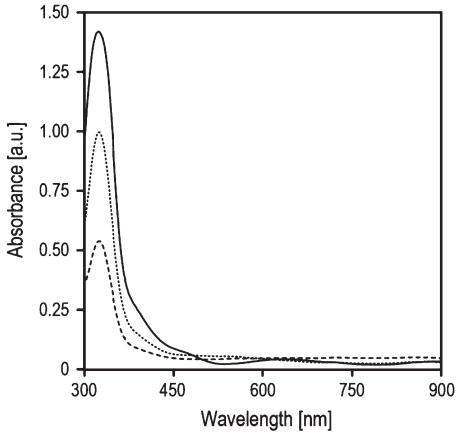

Figure 4. UV/vis spectra of $AuCl_4^-$ loaded PMETAC brushes. The initial PMETAC brush thicknesses were 54 (dashed line), 150 (dotted line), and 315 nm (full line).

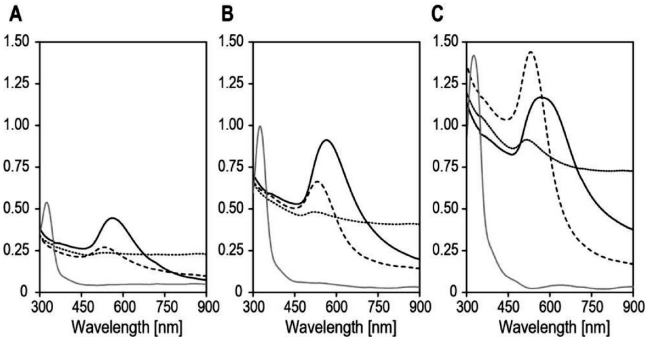

Figure 5. UV/vis spectra of $AuCl_4^-$ loaded PMETAC brushes before (gray lines) and after reduction (black lines) in the presence of 10 mM (full line), 100 mM (dashed line), and 500 mM (dotted line) $NaBH_4$. The experiments were carried out using PMETAC brushes with initial thicknesses of (A) 54, (B) 150, and (C) 315 nm.

which was evidenced by disappearance of the OH stretching band at ~3300 cm^{-1} (Figure 2C). These observations are in agreement with previous reports in which it was shown that counterion exchange of PMETAC brushes with poorly hydrated and large ions can lead to a so-called "hydrophobic collapse".[44] The analysis of AFM cross-sectional profiles of patterned substrates, however, revealed essentially no changes in film thickness upon counterion exchange with $HAuCl_4$ for the thinnest brush, whereas a slight increase in film thickness was observed upon loading 150 and 315 nm thick PMETAC brushes with $HAuCl_4$ (Figure 1 and Table 1). The apparent absence of a significant decrease in film thickness as it may have been expected upon dehydration and hydrophobic collapse is probably related to the fact that the AFM cross-sectional profiles were recorded in air and not under water, as was the case in previously reported studies. Upon exposure to the air, the PMETAC brushes are hydrated to a lesser extent as compared to incubation in water, and as a result the apparent film thicknesses measured in air are likely to be smaller than those measured in water.

The next step in the polymer brush guided fabrication of thin gold films involves reduction of the polymer-brush-immobilized $AuCl_4^-$ to generate a polymer brush−gold nanoparticle (AuNP) composite film. To evaluate the possible influence of gold nanoparticle size on the formation and morphology of the final gold films, the reduction experiments were carried out using different $NaBH_4$ concentrations. The reduction of $AuCl_4^-$ and the formation of gold nanoparticles can be monitored using UV/vis spectroscopy. Figure 5 shows three series of UV/vis spectra of $AuCl_4^-$ and gold nanoparticle loaded films, which were prepared from PMETAC brush-coated glass slides with initial thicknesses

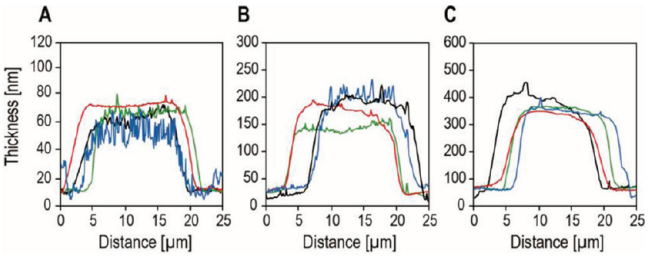

Figure 6. AFM cross-sectional profiles of patterned PMETAC·$AuCl_4$ brushes before (black) and after reduction with 10 (green), 100 (red), and 500 mM (blue) $NaBH_4$ for 30 s. PDMAEMA brushes with initial thicknesses of (A) 37, (B) 99, and (C) 284 nm were used for preparation of these films.

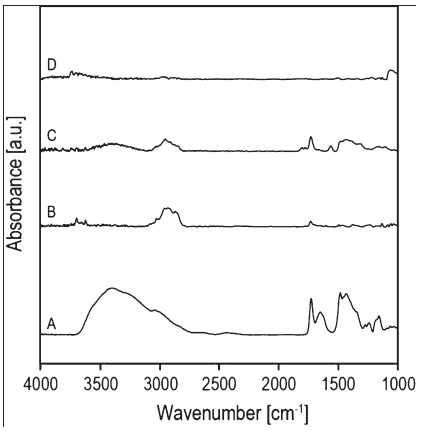

Figure 7. FTIR spectra of (A) a polymer−AuNP composite film prepared from a 150 nm thick PMETAC brush (the absorbed precursor was reduced with 100 mM $NaBH_4$ aqueous solution); (B) the same film as in A, but after two plasma treatment cycles; (C) a polymer−AuNP composite film generated from a 315 nm thick PMETAC brush (same reduction conditions as in A) after two plasma treatment cycles, and (D) the same film as C, but after four plasma treatment cycles.

of 54, 150, and 315 nm. For all three substrates, $NaBH_4$ reduction resulted in disappearance of the UV absorbance at 320 nm and the appearance of a new peak around 520 nm, which is the characteristic gold nanoparticle SPR resonance. The complete disappearance of the peak at 320 nm suggests quantitative reduction of the $AuCl_4^-$ precursor salt. Figure 5 also shows that increasing the concentration of reducing agent leads to broadening of the SPR peak, an increased absorption in the red region and a blue shift of the SPR maximum. While the blue shift of the SPR peak maximum suggests the formation of smaller sized gold nanoparticles as the concentration of reducing agent is increased, the concomitant broadening of the SPR signal reflects the increased tendency of these smaller particles to aggregate.[45] The average diameters of the gold nanoparticles as estimated from the UV−vis spectra are provided in the Supporting Information (Table S1). The AFM cross-sectional profiles in Figure 6 show that in most cases the reduction of $AuCl_4^-$ and the formation of the gold nanoparticles are accompanied by a slight decrease in thickness of polymer brush AuNP composite films.

Finally, the polymer brush−AuNP composite films were subjected to an oxygen plasma treatment to remove the stabilizing polymer matrix and allow coalescence of the gold nanoparticles. The oxygen plasma treatment was performed in consecutive cycles of four minutes so as to maintain the temperature

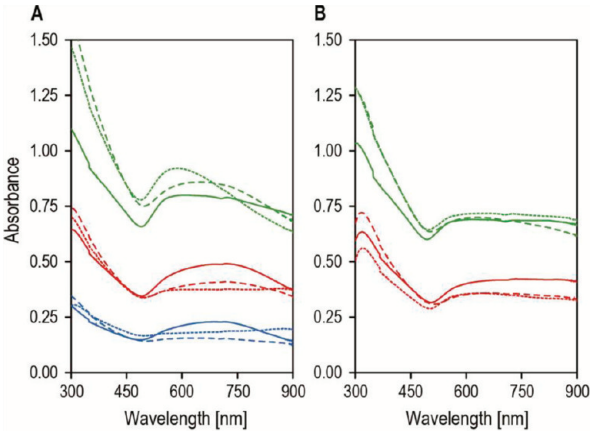

Figure 8. UV/vis spectra of gold films obtained after subjecting PMETAC−AuNP composite films to (A) four and (B) six oxygen plasma treatment cycles. The samples were obtained from PMETAC brush templates with initial thicknesses of 54 (blue line), 150 (red line) and 315 nm (green line). The full, dashed and dotted lines are spectra of samples that were obtained from nanoparticle - brush composite films prepared by reduction of $AuCl_4^-$-loaded PMETAC brushes with 10, 100, and 500 mM $NaBH_4$, respectively.

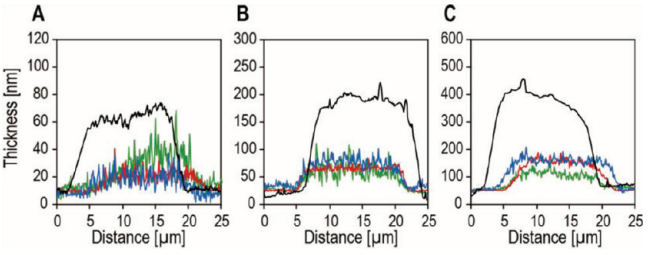

Figure 9. AFM cross-sectional profiles of patterned PMETAC•$AuCl_4$ films (black) and gold films obtained after four oxygen plasma treatment cycles. PDMAEMA brushes with initial thicknesses of (A) 37, (B) 99, and (C) 285 nm were used for these experiments. Prior to oxygen plasma treatment $AuCl_4^-$ loaded polymer brushes were treated with 10 (green lines), 100 (red lines) and 500 mM (blue lines) $NaBH_4$ for 30 s.

in the 50−70 °C range. The degradation of the polymer matrix was monitored using FTIR spectroscopy and is most apparent by following the changes in the ester carbonyl peak at 1730 cm^{-1} (Figure 7). As indicated in Figure 7, subjecting polymer brush−AuNP composite films prepared from 150 and 315 nm thick PMETAC brushes to two plasma treatment cycles already removed a major part of the brush matrix, while four plasma treatment cycles were sufficient to completely remove the brush, as is evident from the FTIR spectrum of the thickest PMETAC−AuNP composite film. Comparison of the UV/vis spectra of the polymer brush−AuNP composite films before (Figure 5) and after plasma treatment (Figure 8) reveals that removal of the polymer matrix is accompanied by a broadening of the gold SPR absorbance and an increased absorbance in the red region of the UV/vis spectra. These effects become more prominent with increasing number of plasma treatment cycles and reflect the increased aggregation of the gold nanoparticles upon removal of the stabilizing polymer brush. Analysis of the AFM height profiles of patterned films revealed a significant decrease in film thickness upon oxygen plasma treatment (Figure 9). Subjecting gold nanoparticle composite films prepared from PMETAC brushes with initial thicknesses of 54, 150, and 315 nm to four oxygen

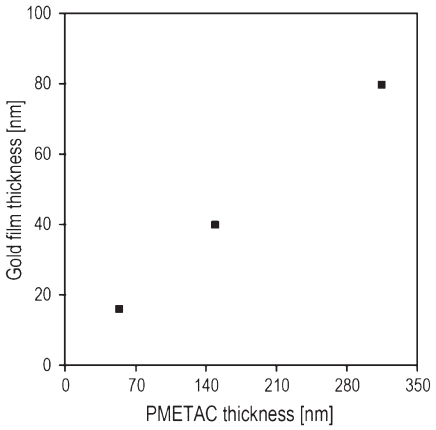

Figure 10. Comparison of the thickness of gold films obtained after plasma treatment of PMETAC−AuNP composite films with that of the original PMETAC brush template. The reported gold film thicknesses refer to films obtained from PMETAC−AuNP composite films prepared by reduction of $AuCl_4^-$-loaded PMETAC brushes with 100 mM $NaBH_4$.

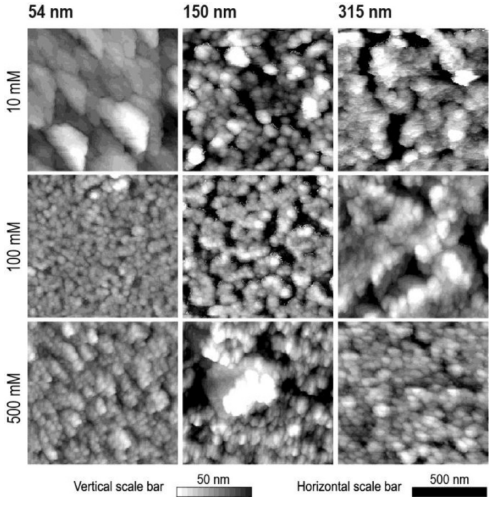

Figure 11. AFM images of gold films prepared from PMETAC-AuNP composite films that were subjected to four plasma treatment cycles. The PMETAC-AuNP composite films were prepared from PMETAC brushes with thicknesses of 54, 150, and 315 nm. The indicated concentrations of 10, 100, and 500 mM refer to the $NaBH_4$ concentration that was used for the preparation of the AuNP composite film.

plasma treatment cycles, for example, affords gold film with thicknesses of about 16, 40, and 80 nm respectively. Figure 10 compares the thickness of the final gold films with that of the original PMETAC brushes. The linear correlation nicely illustrates that the thickness of the gold films can be adjusted by controlling the thickness of the PMETAC brush. More detailed, higher-resolution AFM analysis revealed that the gold films essentially consist of aggregated AuNPs (Figure 11). The surface roughness of the gold films that is evident from the cross-sectional profiles in Figure 9 probably reflects the differences in packing and aggregation behavior of the different sized gold nanoparticles. In addition to providing information on the thickness of the final gold films and demonstrating that variations of the PMETAC brush thickness can be used to direct the thickness of the final gold films, the AFM images also provide

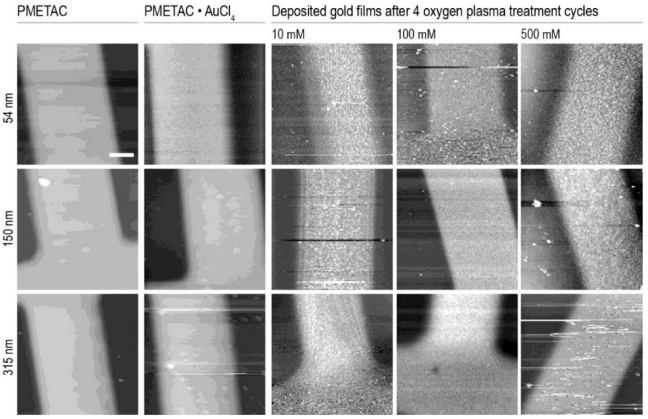

Figure 12. AFM topography images of patterned PMETAC brushes (three different initial thicknesses), $HAuCl_4$-loaded PMETAC brushes, and gold films obtained after four oxygen plasma treatments. The indicated concentrations of 10, 100, and 500 mM refer to the $NaBH_4$ concentration that was used to reduce the gold precursor nanoparticles inside the PMETAC brush template. Scale bar = 5 μm.

evidence for the ability of the PMETAC brushes to guide the lateral deposition and formation of the gold films. This is illustrated by the AFM topography images shown in Figure 12, which demonstrate that the micropatterned template provided by the original PMETAC brush is replicated into the PMETAC−AuNP composite film as well as into the final gold films. This indicates that the precursor gold salt is selectively taken up by the PMETAC brush and does not nonselectively deposit on non-brush covered areas. Closer examination of the gold covered regions of the substrate (see Figure S1 in the Supporting Information) indicated that the gold films, especially when prepared from thinner brushes and using lower $NaBH_4$ concentrations, are relatively free of defects over areas that span multiple micrometers.

XPS analysis indicated that oxygen plasma treatment resulted in the formation of gold oxide and subsequent decomposition of this thermodynamically instable material to gold upon storage.[46−48] This is illustrated in Figure 13, which shows XPS spectra of gold films obtained after 6 plasma treatment cycles, both directly after plasma treatment as well as and 7 and 24 h later. The Au4f high-resolution scan recorded directly after the plasma treatment reveals the presence of a second pair of $Au4f_{7/2}$ and $Au4f_{5/2}$ signals that are slightly shifted to higher energies, which is indicative for the formation of gold oxide. In XPS spectra recorded 7 h after plasma treatment, the characteristic gold oxide signals had already decreased significantly in intensity, and in spectra obtained after 24 h, no evidence for gold oxide could be found, supporting the gradual conversion of the initially formed gold oxide to gold upon storage of the samples. The survey scans in Figure 13 also show a small C1s signal. The high-resolution scans, which are included in the Supporting Information, suggest that these are probably due to carbon contaminations rather than to residual polymer brush (Figure S2).

Preparation of Pd/Au Bimetallic Films. In a final experiment, it was attempted to extend the concept discussed above to the fabrication of bimetallic films. The basic concept is outlined in Scheme 2 and involves loading of a PMETAC brush template with a first precursor salt (here: $PdCl_4^{2-}$), followed by incubation of this loaded brush in a solution containing a second precursor salt (here: $AuCl_4^-$) to allow ion exchange and form a

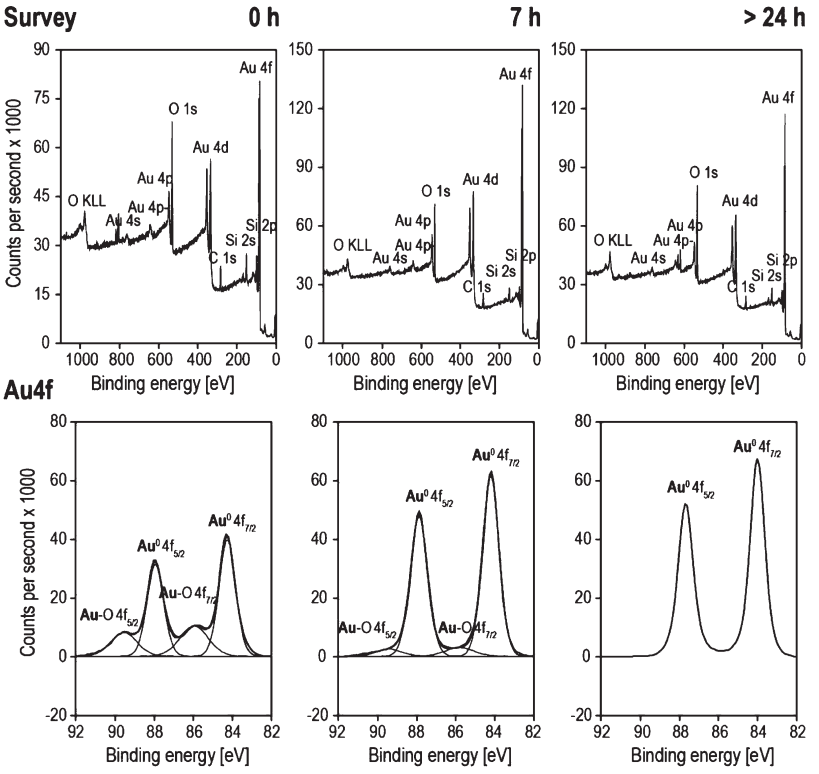

Figure 13. XPS survey scans and Au4f high-resolution spectra of gold films produced from a 150 nm thick PMETAC polymer brush template analyzed directly (left column), 7 h (middle column) and 24 h (right column) after the 6th oxygen plasma treatment cycle.

Scheme 2. Polymer Brush Guided Preparation of Palladium/Gold Bimetallic Films

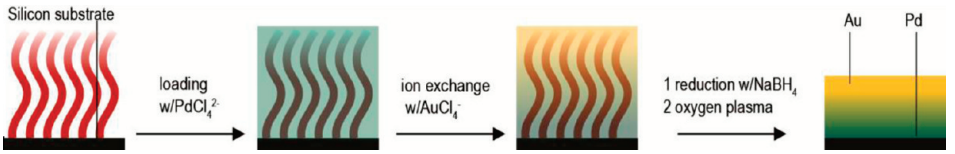

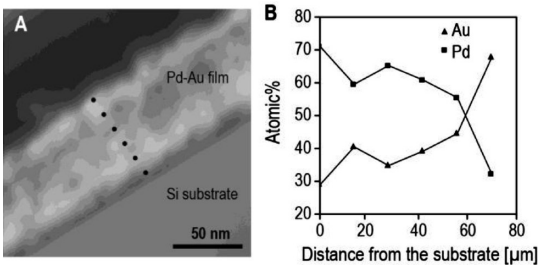

Figure 14. (A) cross-sectional TEM image of a Pd/Au bimetallic film. The dots of the TEM image indicate the spots that were used for EDX analysis. (B) relative atomic% of Pd and Au in the Pd/Au bimetallic film as a function of the distance of the substrate as determined using EDX spectroscopy.

brush loaded with two different layers of metal ion precursors. In a final step, the metal salt loaded brush is first treated with $NaBH_4$ and then subjected to an oxygen plasma to generate desired palladium/gold bimetallic film.

For a first proof of concept of the strategy outlined in Scheme 2, a 315 nm thick PMETAC brush was first loaded with $PdCl_4^{2-}$ and subsequently exposed to a $HAuCl_4$ solution for two hours to allow anion exchange and incorporation of $AuCl_4^-$ in the brush template. The metal precursor salt loaded brush was subsequently treated with $NaBH_4$ and then subjected to an oxygen plasma treatment. To investigate the structure of the resulting bimetallic film, the sample was cross-sectioned by means of mechanical polishing and analyzed by energy-dispersive X-ray (EDX) spectroscopy (Figure 14). Figure 14A shows a cross-sectional TEM image of the bimetallic film and Figure 14B plots the relative concentrations of Pd and Au as obtained from the EDX analysis as a function of the distance from the substrate. The EDX results indicate that the bimetallic film does not consist of two layers. Instead, the strategy outlined in Scheme 2 results in a gradient-type palladium/gold bimetallic film, which is enriched in Pd near the silicon substrate and rich in gold at the top of the film.

CONCLUSIONS

In this contribution, we have demonstrated the feasibility of polymer brushes grown via surface-initiated atom transfer radical polymerization to guide the formation of thin gold films. Gold

films with thicknesses between 16 and 80 nm were obtained by loading PMETAC brushes with $HAuCl_4$ followed by $NaBH_4$ reduction to generate a polymer brush-gold nanoparticle composite film. A final oxygen plasma treatment removed the stabilizing polymer brush matrix and resulted in the formation of a thin gold film. The thickness of the gold film was found to scale linearly with the thickness of the polymer brush template. By exposing the polymer brush template not to a single metal precursor salt, but successively to Na_2PdCl_4 and $HAuCl_4$, the concept could be extended to the preparation of bimetallic films. EDX analysis revealed that these bimetallic films do not consist of two distinct, separate layers, but instead are gradient films that are enriched in the first component (here: palladium) near the substrate and rich in the other component (here: gold) at the top of the film. The polymer-brush-guided film formation strategy outlined in this contribution represents an interesting alternative to other chemical-solution routes and may be extended to a variety of other metals and metal oxides. Because the polymer brush template can be prepared with precise control of both thickness as well as in terms of lateral dimensions via the use of appropriate patterning techniques, the proposed strategy could open the door to a broad variety of thin metal films with complex composition profiles and microstructures.

■ ASSOCIATED CONTENT

Supporting Information. Additional characterization data on gold nanoparticle sizes, AFM images, and high-resolution C 1s XPS spectra of gold films (PDF). This information is available free of charge via the Internet at http://pubs.acs.org.

■ AUTHOR INFORMATION

Corresponding Author

*E-mail: harm-anton.klok@epfl.ch. Fax: + 41 21 693 5650. Tel.: + 41 21 693 4866.

■ ACKNOWLEDGMENT

The authors thank Caroline Calderone and Danièle Laub from the Centre Interdisciplinaire de Microscopie Electronique (CIME, EPFL) for their help regarding the TEM sample preparation, imaging and analysis, Nicolas Xanthopoulos (CIME, EPFL) for his support with the XPS experiments and Dr. Christopher Plummer (LTC, EPFL) for his help with the AFM experiments.

■ REFERENCES

(1) Freund, H.-J.; Pacchioni, G. *Chem. Soc. Rev.* **2008**, *37*, 2224–2242.
(2) Gray, J. E.; Luan, B. *J. Alloys Compd.* **2002**, *336*, 88–113.
(3) Leskelä, M.; Ritala, M. *Thin Solid Films* **2002**, *409*, 138–146.
(4) Hantschel, T.; Wong, L.; Chua, C. L.; Fork, D. K. *Microelectron. Eng.* **2003**, *67−8*, 690–695.
(5) Inberg, A.; Shacham-Diamand, Y.; Rabinovich, E.; Golan, G.; Croitoru, N. *J. Electron. Mater.* **2001**, *30*, 355–359.
(6) Ali, M.; Wang, C. Y.; Röhlig, C. C.; Cimalla, V.; Stauden, T.; Ambacher, O. *Sens. Actuators, B* **2008**, *129*, 467–472.
(7) Yeh, W.-H.; Kleingartner, J.; Hillier, A. C. *Anal. Chem.* **2010**, *82*, 4988–4993.
(8) Singhal, S. C. *Solid State Ionics* **2000**, *135*, 305–313.
(9) O'Regan, B.; Grätzel, M. *Nature* **1991**, *353*, 737–740.
(10) Hendricks, J. H.; Aquino, M. I.; Maslar, J. E.; Zachariah, M. R. *Chem. Mater.* **1998**, *10*, 2221–2229.
(11) Hultman, L.; Sundgren, J. E.; Greene, J. E.; Bergstrom, D. B.; Petrov, I. *J. Appl. Phys.* **1995**, *78*, 5395–5403.
(12) Brown, I. G. *Annu. Rev. Mater. Sci.* **1998**, *28*, 243–269.
(13) Sondag-Huethorst, J. A. M.; Fokkink, L. G. J. *Langmuir* **1995**, *11*, 4823–4831.
(14) Kim, Y.; Miyauchi, K.; Ohmi, S.; Tsutsui, K.; Iwai, H. *Microelectron. J.* **2005**, *36*, 41–49.
(15) Elshabini-Riad, A.; Barlow, F. D., III. *Thin Film Technology Handbook*; McGraw-Hill: New York, 1998.
(16) Smith, L. D., *Thin Film Deposition*. McGraw-Hill: New York, 1995.
(17) Hrapovic, S.; Liu, Y. L.; Enright, G.; Bensebaa, F.; Luong, J. H. T. *Langmuir* **2003**, *19*, 3958–3965.
(18) Hu, J. D.; Wei, L. B.; Jian, C. B.; Zhang, X. H.; Zhao, X. Y. *Surf. Coat. Technol.* **2008**, *202*, 2922–2926.
(19) Azzaroni, O.; Zheng, Z. J.; Yang, Z. Q.; Huck, W. T. S. *Langmuir* **2006**, *22*, 6730–6733.
(20) Gao, Y. R.; Liu, C. M.; Fu, S. L.; Jin, J.; Shu, X.; Gao, Y. H. *Surf. Coat. Technol.* **2010**, *204*, 3629–3635.
(21) Lange, F. F. *Science* **1996**, *273*, 903–909.
(22) Kowalczyk, B.; Byrska, M.; Mahmud, G.; Huda, S.; Kandere-Grzybowska, K.; Grzybowski, B. A. *Langmuir* **2009**, *25*, 1905–1907.
(23) Girotto, C.; Rand, B. P.; Steudel, S.; Genoe, J.; Heremans, P. *Org. Electron.* **2009**, *10*, 735–740.
(24) Gotesman, G.; Naaman, R. *Langmuir* **2008**, *24*, 5981–5983.
(25) Jia, Q. X.; McCleskey, T. M.; Burrell, A. K.; Lin, Y.; Collis, G. E.; Wang, H.; Li, A. D. Q.; Foltyn, S. R. *Nat. Mater.* **2004**, *3*, 529–532.
(26) Burrell, A. K.; McCleskey, M. T.; Jia, Q. X. *Chem. Commun.* **2008**, 1271–1277.
(27) Li, X.; Huang, F.; Curry, M.; Street, S. C.; Weaver, M. L. *Thin Solid Films* **2005**, *473*, 164–168.
(28) Wong, K. W.; Sin, L. Y.; Yeung, M. K.; Hark, S. K.; Lau, W. M. *Appl. Phys. A: Mater. Sci. Process.* **2007**, *87*, 23–26.
(29) Barbey, R.; Lavanant, L.; Paripovic, D.; Schüwer, N.; Sugnaux, C.; Tugulu, S.; Klok, H.-A. *Chem. Rev.* **2009**, *109*, 5437–5527.
(30) Yang, S. H.; Kang, K.; Choi, I. S. *Chem.-Asian J.* **2008**, *3*, 2097–2104.
(31) Kim, D. J.; Lee, K. B.; Lee, T. G.; Shon, H. K.; Kim, W. J.; Paik, H. J.; Choi, I. S. *Small* **2005**, *1*, 992–996.
(32) Kim, D. J.; Lee, K.-B.; Chi, Y. S.; Kim, W.-J.; Paik, H.-J.; Choi, I. S. *Langmuir* **2004**, *20*, 7904–7906.
(33) Tugulu, S.; Harms, M.; Fricke, M.; Volkmer, D.; Klok, H.-A. *Angew. Chem., Int. Ed.* **2006**, *45*, 7458–7461.
(34) Azzaroni, O.; Brown, A. A.; Cheng, N.; Wei, A.; Jonas, A. M.; Huck, W. T. S. *J. Mater. Chem.* **2007**, *17*, 3433–3439.
(35) Cheng, Z.; Zhang, L.; Zhu, X.; Kang, E. T.; Neoh, K. G. *J. Polym. Sci., Part A: Polym. Chem.* **2008**, *46*, 2119–2131.
(36) Yu, K.; Wang, H. F.; Han, Y. C. *Langmuir* **2007**, *23*, 8957–8964.
(37) Benetti, E. M.; Sui, X. F.; Zapotoczny, S.; Vancso, G. J. *Adv. Funct. Mater.* **2010**, *20*, 939–944.
(38) Calvo, A.; Fuertes, M. C.; Yameen, B.; Williams, F. J.; Azzaroni, O.; Soler-Illia, G. J. A. A. *Langmuir* **2010**, *26*, 5559–5567.
(39) Gupta, S.; Agrawal, M.; Conrad, M.; Hutter, N. A.; Olk, P.; Simon, F.; Eng, L. M.; Stamm, M.; Jordan, R. *Adv. Funct. Mater.* **2010**, *20*, 1756–1761.
(40) Schüwer, N.; Klok, H.-A. *Adv. Mater.* **2010**, *22*, 3251–3255.
(41) Plamper, F. A.; Schmalz, A.; Penott-Chang, E.; Drechsler, M.; Jusufi, A.; Ballauff, M.; Müller, A. H. E. *Macromolecules* **2007**, *40*, 5689–5697.
(42) Minelli, C.; Hinderling, C.; Heinzelmann, H.; Pugin, R.; Liley, M. *Langmuir* **2005**, *21*, 7080–7082.
(43) Sanjuan, S.; Perrin, P.; Pantoustier, N.; Tran, Y. *Langmuir* **2007**, *23*, 5769–5778.
(44) Azzaroni, O.; Brown, A. A.; Huck, W. T. S. *Adv. Mater.* **2007**, *19*, 151–154.
(45) Ghosh, S. K.; Pal, T. *Chem. Rev.* **2007**, *107*, 4797–4862.
(46) Ron, H.; Rubinstein, I. *Langmuir* **1994**, *10*, 4566–4573.
(47) Koslowski, B.; Boyen, H.-G.; Wilderotter, C.; Kästle, G.; Ziemann, P.; Wahrenberg, R.; Oelhafen, P. *Surf. Sci.* **2001**, *475*, 1–10.
(48) Lim, D. C.; Lopez-Salido, I.; Dietsche, R.; Bubek, M.; Kim, Y. D. *Angew. Chem., Int. Ed.* **2006**, *45*, 2413–2415.